 doi:10.20944/preprints202009.0442.v1

Article

Refinement on the Solidification Structure of H13 tool steel under Multi-Rotational Speeds Super-Gravity Field

SHAO-YING LI[1,2], SHU-YANG QIN[1], XIAO-JUN XI[1,2], GUAN-YONG SUN[1,2], WEN-SHENG YANG[1,2], JING GUO[1,2] and HAN-JIE GUO[1,2,3*]

1.—School of Metallurgical and Ecological Engineering, University of Science and Technology Beijing, 30 Xueyuan Road, Haidian District, Beijing 100083, People's Republic of China.
2.—Beijing Key Laboratory of Special Melting and Preparation of High-End Metal Materials, Beijing 100083, People's Republic of China.
* Correspondence:.—e-mail: guohanjie@ustb.edu.cn

In this paper, the effect of multi-rotational speeds super-gravity field on the grain refinement and tensile properties of as-cast H13 steel were investigated systematically. The experimental results revealed that the as-cast grains of H13 steel can be significantly refined in multi-rotational speeds supergravity field. In conventional supergravity field, with the decrease of rotational radius, the secondary dendrite average spacing (SDAS) and the austenite grain average size (AGAS) increase, and the maximum values of SDAS and AGAS are 90 μm and 55 μm, respectively. while in multi-speeds supergravity fields, at the range of increasing rotational speeds, SDAS and AGAS decrease as the rotational radius decreases. In three-rotational speeds supergravity field, the maximum values of SDAS and AGAS are 80 μm and 50 μm. In five-rotational speeds supergravity field, the maximum values of SDAS and AGAS are reduced to 58 μm and 34 μm. Accordingly, both the tensile strength and the plasticity are enhanced with the increasing the number of rotational speeds in supergravity field, especially for the inner position of supergravity sample. The ultimate tensile strengths at outer, middle, and inner positions of H13 steel solidified in conventional supergravity field are 1445 MPa, 1378 MPa, and 1023 MPa, corresponding elongations of 2%, 1.5%, and 0.5%, while in the five-rotational speeds supergravity field, they are 1408 MPa, 1443 MPa, and 1453 MPa, corresponding elongations of 1.8%, 3.9%, and 2.2%. The mechanism for the grain refinement is that multi-speeds super-gravity can reduce the critical nucleation work of austenite, and the tangential force produced by changing the rotational speeds breaks dendrites at the solidification front, refining solidification structure.

Keywords: refinement mechanisms; solidification structure; multi-rotational speeds super-gravity field

1.Introduction

H13 hot work die steel is widely used in extrusion, die casting, hot forging and other industries due to its high strength, high hardness, high toughness and temper softening [1,2]. Because of the ripening phenomenon during solidification, the solidification structure of H13 steel coarsens with the increase of time [3]. The coarsening solidification structure leads to casting defects such as segregation, shrinkage and microcracking, which severely degrades the performance of the product [4,5]. Many scholars have done a lot of research on the method of refining the solidification structure. The traditional methods include optimizing melting, changing casting process and adding nucleating agent. There are also new methods such as applying an electric field [6], a magnetic field [7], an ultrasonic field [8], and a super-gravity field [9]. In particular, the refinement method of applying a super-gravity field has the advantages of low cost, low pollution and strong operability. For the study of super-gravity solidification structure, most scholars focus on the influence of casting temperature,

 doi:10.20944/preprints202009.0442.v1

the effective solidification stage of super-gravity, casting material, super-gravity coefficients and other factors [9,10].

Zhao et al. have investigated the influence of super-gravity field on aluminum grain refining, and concluded that the grain size decreased rapidly as the gravity coefficient from 1 to 250, and then remained nearly unchanged from 250 to 1000. However, their study is limited to the equiaxed crystal region in the middle of the sample, and lacks the change of crystal grains along the direction of super-gravity [11]. In another study, Yang et al. studied the microstructures of Al-Cu alloys containing the eutectic phase (Al_2Cu+α-Al) and α-Al matrix at different positions of the samples in super gravity fields. The found that when Al-Cu alloys were solidified in super gravity field, the eutectic phase increases along the direction of super gravity field. In other words, the refinement of α-Al at the up area is worse than that at the bottom area [12]. This phenomenon also appeared in the supergravity samples of Cu-Sn alloys [13].

In order to further refine the solidification structure at the upper area in the supergravity sample, many researchers have discussed the refinement mechanisms of different alloys in the supergravity field. Zhao et al. proposed that under the super-gravity, the dendrites are broken, and more nucleation sites are provided (i.e. heavy crystal rain mechanism). The theory is the refinement mechanism of industrial pure aluminum solidification structure in the super-gravity field, but the smaller critical nucleation work, directly caused by super-gravity, did not contribute to grain refining [11]. Melgarejo et al. found that the super-gravity can increase the cooling rate of the melt and refine the solidification structure of Al-Mg-B alloy [14]. Under the super-gravity field with the constant rotational speed, the smaller critical nucleation work contributed to refining the solidification structure of ZCuSn3Zn8Pb6NiFeCo alloys [15].

Based on these refinement mechanisms, researchers proposed the improvement measures of increasing the supergravity coefficient and changing the stage of applying supergravity. Compared with the sample before improvement, the solidification structure has a certain degree of refinement, but the solidification structure at up area still cannot be effectively refined, which accounts for about a quarter of the sample [11-13]. Due that super-gravity technology was limited by the experimental apparatus, these researches related to structure refinement in supergravity field are mainly conducted in laboratory-scale experiments, and the obtained samples are all less than 200 g. If the super-gravity refinement method in literatures is applied to the industrial-grade steel ingots above 30 kg, the refining effect at the upper area of the ingot will be even worse. In addition, the low-melting temperature metal, such as Al-Cu alloys and Cu-Sn alloys was used in early research, and the higher-melting temperature metals (e.g. steel) were not payed attention. Therefore, it is very necessary to explore a new supergravity method suitable for refining the solidification structure of the entire industrial-grade steel ingot.

In the present article, the effect of supergravity on the solidification structure and tensile properties of H13 tool steel was investigated by industrial experiments under the conventional supergravity field and the supergravity field with multiple rotational speeds defined as “the multi-rotational speeds supergravity field”. Furthermore, by applying different supergravity fields during solidification of H13 steel, the refining mechanism was revealed experimentally and discussed. The research result provides a theoretical basis for the refining solidification structure of H13 steel industrial ingot by supergravity.

2. Experimental Procedures

The composition of H13 tool steel is shown in Table 1. The electrode of H13 was placed in a 50 kg electroslag crucible furnace to obtain molten steel. The slag in electroslag crucible was a mixture of 60 wt% CaF_2, 20 wt% CaO and 20 wt% Al_2O_3 to prevent oxidation of molten steel as much as possible during the experiment.

Table 1. Chemical composition of the H13 tool steel (wt.%).

C	Si	Mn	Cr	Mo	V	Al	W	O	N	Fe
0.46	0.9	0.3	4.6	1.4	0.9	0.03	0.02	0.0025	0.0104	Bal.

Preprints (www.preprints.org) | NOT PEER-REVIEWED | Posted: 18 September 2020 doi:10.20944/preprints202009.0442.v1

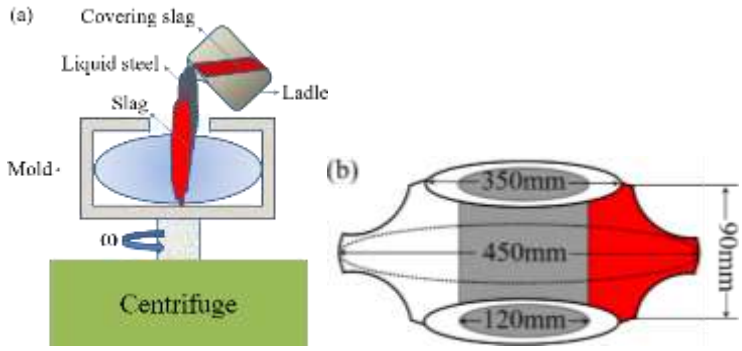

Figure 1. Schematic diagram of super-gravity apparatus (b) Schematic diagram of super-gravity casting.

The super-gravity device is shown in Fig. 1(a). The inner size of the cast iron mold is approximately D×H=450 mm×90 mm. The super-gravity experiment was performed at room temperature (25 ℃). The molten metal (35 kg) and slag (7 kg) at a temperature of 1923 K were poured into a rotating mold with the rotational speed of 500 r/min. The mixture of steel and slag was completely poured into the mold within 10 seconds, and the entry sequence is a small amount of slag, the mixture of slag and molten steel and the remaining slag in the furnace. The remaining slag in the furnace is poured into the mold to ensure that the direction of solidification of the molten steel is from the outside to center of the centrifuge. The speed parameters and sample numbers of different supergravity experiments are shown in Table 2. Sample A is solidified in a traditional supergravity field, and Samples B and C are solidified in multi-rotational speeds supergravity fields.

Table 2. Rotational speed($r \cdot min^{-1}$) and time (min) of each stage during supergravity solidification.

No.	First stage speed/Time	Second stage speed/Time	Third stage speed/Time	Fourth stage speed/Time	Fifth stage speed/Time
A	500/8.2				
B	500/0.2	600/4	750/4		
C	500/0.2	600/2	750/2	850/2	950/2

For the samples under super-gravity fields, the cooling rate for all the samples was ranged from 3 ℃/s to 5 ℃/s. The apparatus was kept under operation until the sample is completely solidified, after which the super-gravity apparatus was turned off. The sample was taken out of the mold and immediately covered with insulation cotton to avoid cracks.

The macrostructures of the supergravity ingots were obtained from the vertical section of samples (as shown the red cross section in Fig. 1(b)). All surfaces were mechanically flattened and polished, followed by chemical etching with a solution of HCl (150 mL) + H_2O (150 mL). The samples were chemically etched in a solution of HNO_3 (4 mL) + absolute ethanol (96 mL) for 30 seconds to reveal the dendritic structures and the original austenite grains. The secondary dendrite arm spacing (SDAS) and the average diameter of the austenite grains were measured based on multiple optical micrographs (OM; Leica-DM4M) using the linear intercept method.

In order to study the effects of super-gravity field on tensile properties of H13 steel, tensile tests were performed using an electronic universal testing machine (CMT4105) with the standard of GB/T228.1-2010 at room temperature. Fig. 2 (a) shows the testing specimen with 1.2 mm thickness. The sampling positions of tensile samples in Samples A, B, and C are shown in Fig. 3(b), which are defined as outer, middle and inner. Three parallel test specimens at the same position were taken from each sample, and the distance between two adjacent positions in each sample is 45 mm.

Preprints (www.preprints.org) | NOT PEER-REVIEWED | Posted: 18 September 2020 doi:10.20944/preprints202009.0442.v1

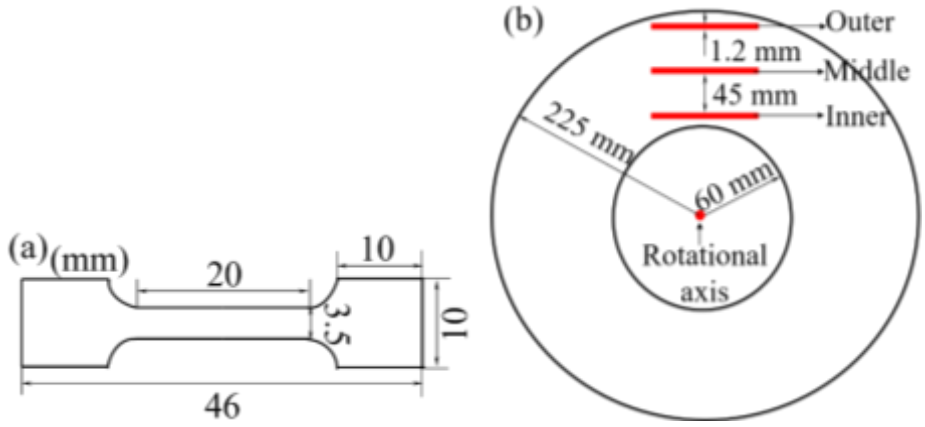

Figure 2. Schematic diagram of the testing specimen (a) Sample size; (b) Sampling positions.

The gravity coefficient [10] is the ratio of super-gravitational acceleration to the normal-gravitational acceleration and can be expressed as Eq. (1).

$$G = \frac{\sqrt{g^2 + (\omega^2 R)^2}}{g} = \frac{\sqrt{g^2 + (\frac{N^2 \pi^2 R}{900})^2}}{g} \quad (1)$$

where, G is the gravity coefficient, ω is the angular speed (rad/s), N is the rotational speed (r/min), R is the distance between the centrifugal axis and the observation position (i.e. rotational radius, m), g is the normal-gravitational acceleration (9.8 m/s²).

3. Results and Discussion

3.1. Macro- and Micro-structures of As-cast H13 Samples in Supergravity Fields

The macro-structure of as-cast H13 steel samples obtained with different supergravity fields in Fig. 3. In order to study the influence of different supergravity fields on the solidification structure of the castings at different positions, the observation area of the solidification structure is selected as shown in Fig. 3(a). The macro-structure in observation area for Samples A, B, and C is shown in Fig. 3(b). For Sample A, there is orderly arranged columnar crystals at Position 1, obvious hollow at Position 2, and center porosity between Position 1 and Position 2. Compared with Sample A, there is no obvious hollow and center porosity for Samples B and C. The possible reason is that during the solidification of Samples B and C, the number of rotational speeds in the supergravity field is increased, which makes the forced feeding effect of centrifugal force stronger. In addition, the macro-structures at Position 1 for Samples B and C are finer than that for Sample A. At Position 2, there are coarse columnar crystals for Sample B, and small columnar crystals for Sample C, which could result from the change in the rotational speeds in the supergravity field at the late solidification stage of Sample C.

Preprints (www.preprints.org) | NOT PEER-REVIEWED | Posted: 18 September 2020 doi:10.20944/preprints202009.0442.v1

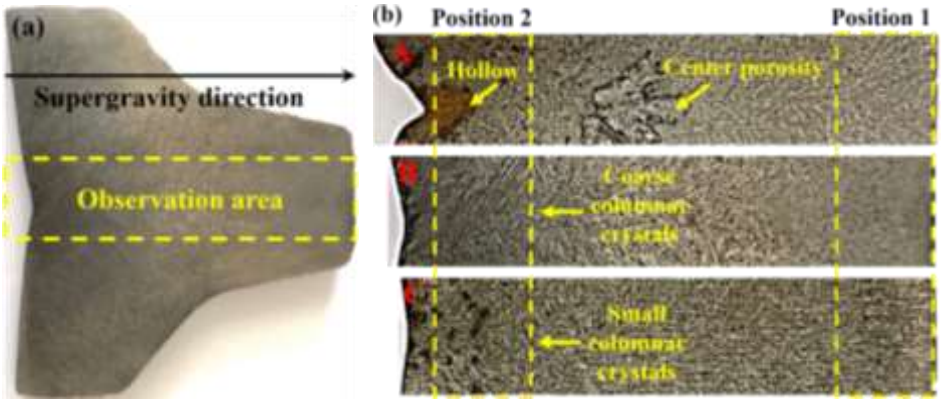

Figure 3. Macro-structure of as-cast H13 steel samples obtained in conventional supergravity and composite super-gravity fields: (a) Schematic diagram of observation area of (b); (b) Macro-structure at different positions in the observation area of Samples A, B and C.

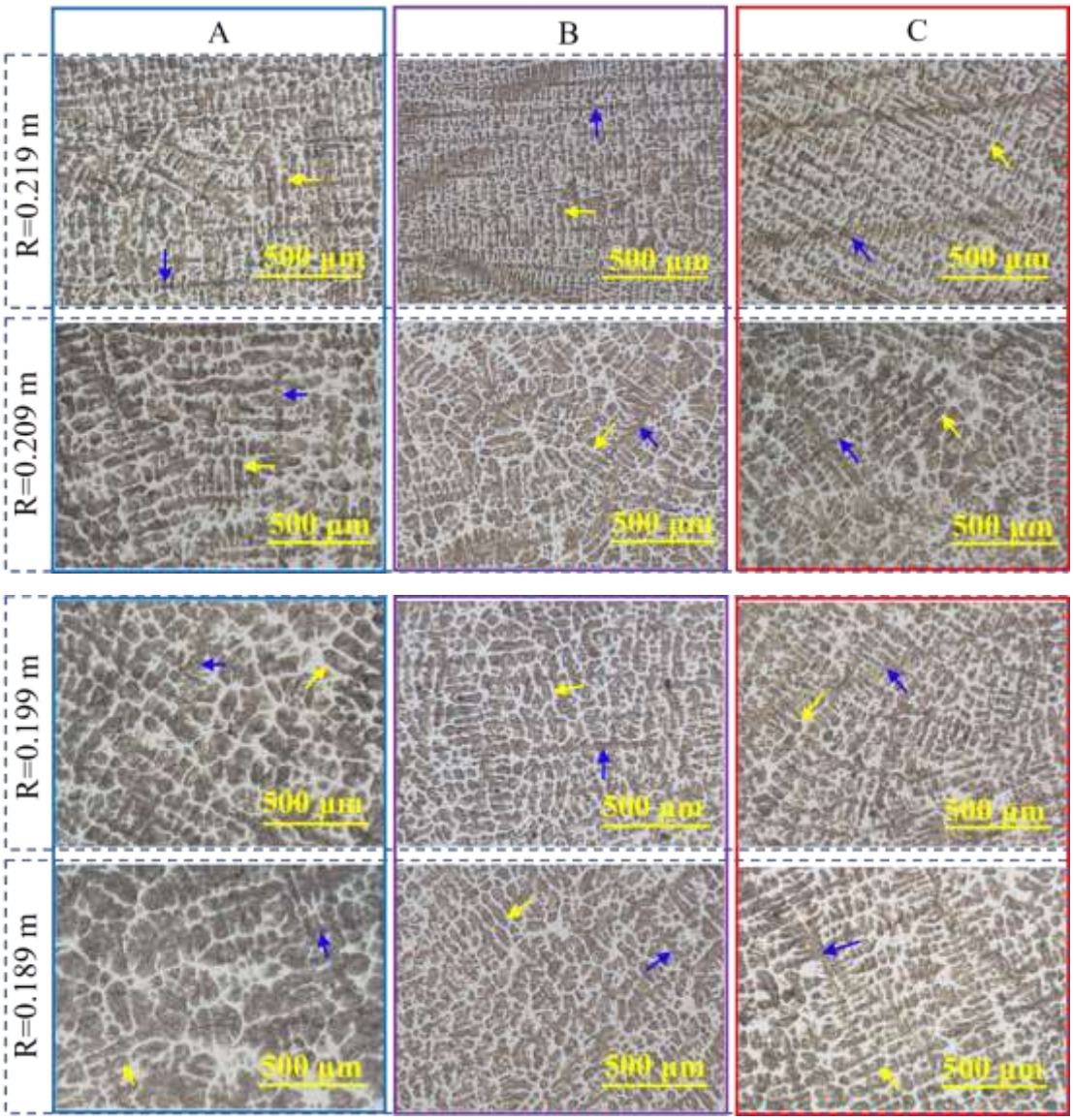

Preprints (www.preprints.org) | NOT PEER-REVIEWED | Posted: 18 September 2020 doi:10.20944/preprints202009.0442.v1

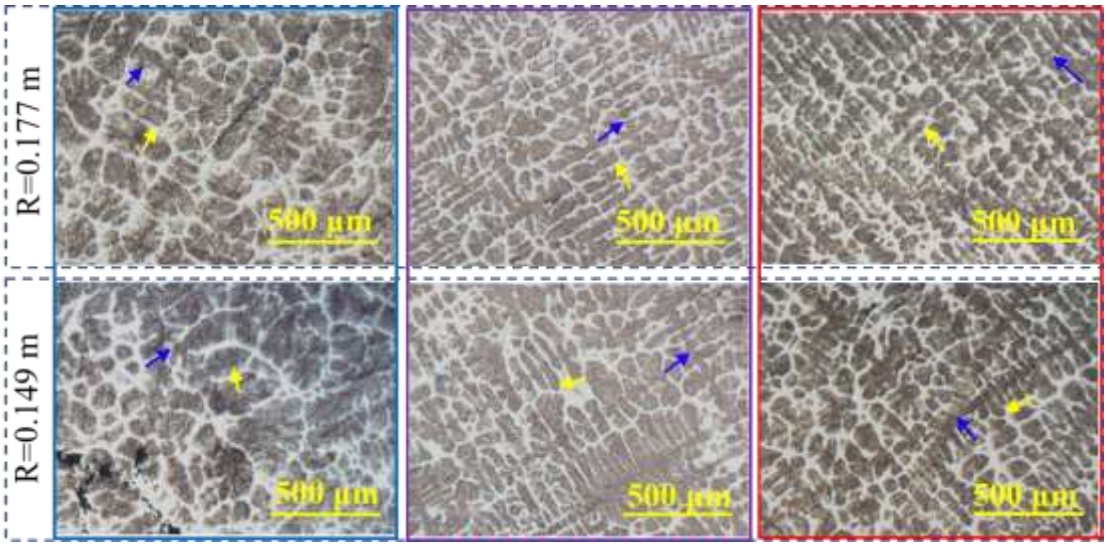

Figure 4. Dendrites structures at different locations in the longitudinal section of Samples A, B, and C (Notes: The blue arrow points to the primary dendrite, the yellow arrow points to the secondary dendrite).

Fig. 4 shows the dendrites structures at different locations in the longitudinal section of the samples. It can be found from Fig. 4 that the primary dendrite spacings and the secondary dendrite spacings of Sample A increase with the decrease of R. The crystals are so developed dendritic morphology that an entire dendrite structure cannot be fully included in a picture at the position of R=0.149 m. When the supergravity field contains three rotational speeds (i.e. Sample B), both the primary and the secondary dendrite size decrease apparently at the range of 0.149 m<R< 0.199 m compared with that of Sample A. When the number of rotational speeds in the supergravity field is increased to five, the dendrites structure is further refined especially for the range of 0.149 m<R< 0.209 m, illustrating that the increase in the number of rotational speeds can greatly refine the solidification structure of as-cast H13 steel in super-gravity field.

Accord to the observation of the prior austenite grains at different positions for Samples A, B, and C, it can be found that in the supergravity field with constant rotational speed, the grain size of austenite increases with the decrease of R. When the number of rotational speeds increases during the solidification under supergravity field, the prior austenite grains decrease apparently, especially for the range of R<0.199 m. Fig. 5 shows the typical prior austenite grains at R=0.149 m of the as-cast H13 samples in three supergravity fields. As shown in Fig. 5, in a picture at the magnification of 500×, there is more prior austenite grains in Sample B and C than in Sample A. On the whole, the prior austenite size decreases with increasing the number of rotational speeds in supergravity field.

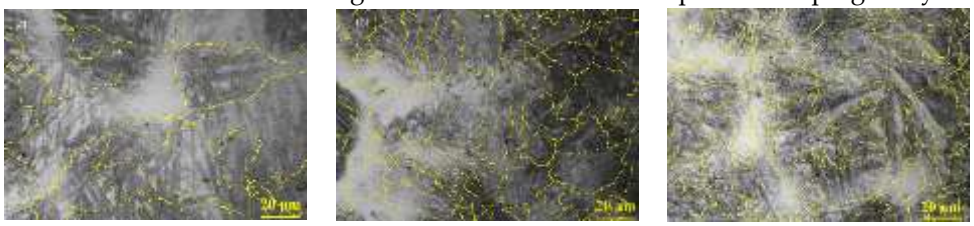

Figure 5. Austenite grains at R=0.149 m in the longitudinal section of the samples (Notes: the yellow curve in the Fig. shows the austenite grain boundary).

In order to further explore the influence of supergravity field on the refinement of solidification structure, Fig. 6 (a) and (b) summarize the average secondary dendrites spacings (i.e. SDAS) and the average austenite grain sizes of the samples obtained in super-gravity fields, respectively. Fig. 6 (c) shows the supergravity coefficients at different positions in the three supergravity fields. It can be seen that when in gravity field with constant rotational speed (i.e. Sample A), with the decrease of R,

 doi:10.20944/preprints202009.0442.v1

the supergravity coefficient decreases, and SDAS and the average grain sizes increase. The minimum values of the secondary dendrite spacing and average grain size appear at R = 0.225 m, which are 40 μm and 27 μm, respectively, and the corresponding supergravity coefficient is 62. When R decreases to 0.152 m, the coefficient of supergravity decreases to 42, and SDAS and the average grain sizes reach their own maximum values which are 92 μm and 55 μm, respectively. This illustrates that the increase in the supergravity coefficient is beneficial to the refinement of solidification structure, which is consistent with the opinion of Yang et al. When in supergravity fields of G=100, 300, and 600, the average grain sizes of as-cast Cu-11wt%Sn are 0.35 μm, 0.173 μm, and 0.074 μm [13].

However, the relationship between the refinement of solidification structure and the supergravity coefficient in Sample A is not is not fully applicable to Sample B and Sample C. When the rotational speed increases during the solidification in supergravity field, with the decrease of R, the secondary dendrite spacings and the austenite grain sizes decrease. For example, in sample B, the secondary dendrite spacings and the grain sizes decreased from 68 μm and 39 μm at R=0.184 m to 51 μm and 32 μm at R=0.176 m. It can be found that from Fig. 6 the maximum values of the secondary dendrite spacing and the grain sizes in sample B are 85 μm and 49 μm at R=0.152 m, and the minimums are 38 μm and 26μm at R=0.219 m. Similarly, when the number of rotational speeds in the supergravity field is increased to five, compared with Samples A and B, the secondary dendrite spacings and grain sizes in sample C are significantly decreased. In Sample C, the maximum values of the secondary dendrite spacing and the average grain size are decreased to 58 μm and 37 μm, respectively, which makes the solidification structure of the entire sample significantly refined. As a whole, compared with the traditional supergravity field, the multi-rotational speeds supergravity field is more conducive to refine the solidification structure of as-cast H13 steel.

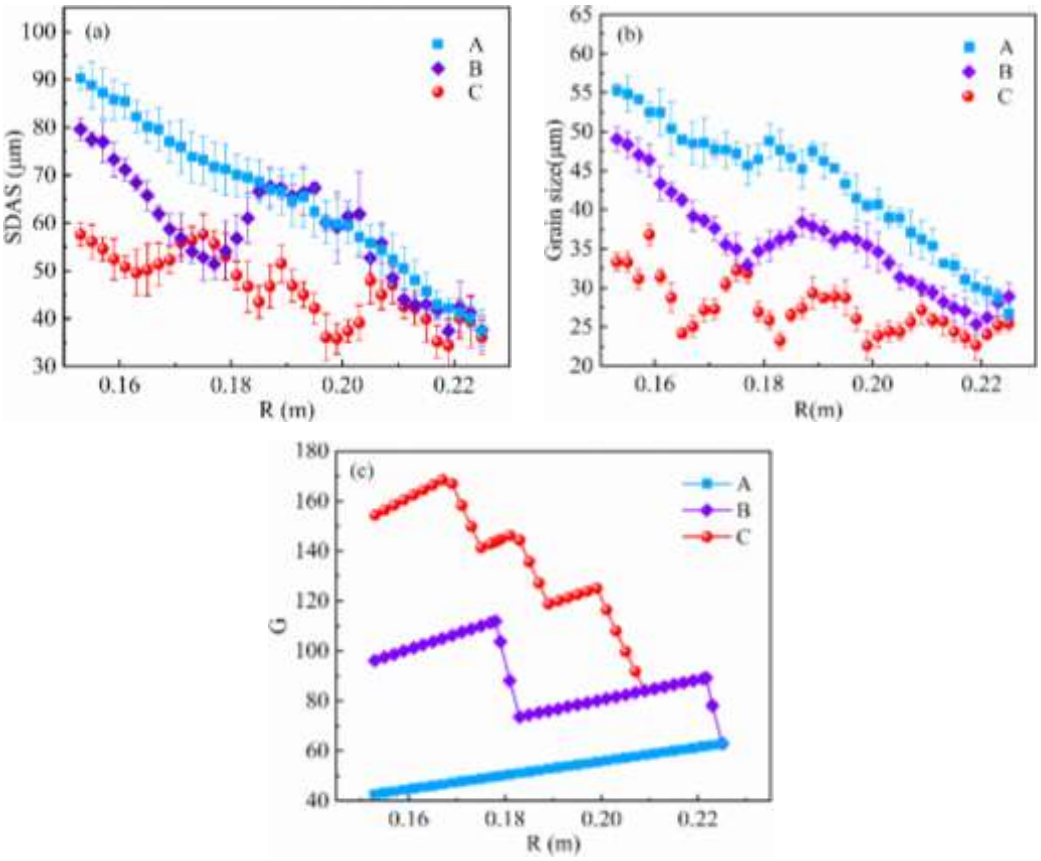

Figure 6. (a) SDAS, (b) Grain size, and (c) supergravity coefficients of different samples solidified in conventional supergravity field and multi-speed supergravity fields.

3.2. The refinement mechanism of H13 solidification structure in supergravity field

In Section 3.1, it can be found that in Samples B and C, the secondary dendrite spacings and the average grain sizes at multiple locations are the same, but the supergravity coefficient is different.

Preprints (www.preprints.org) | NOT PEER-REVIEWED | Posted: 18 September 2020 doi:10.20944/preprints202009.0442.v1

For example, in Sample C, the average grain size is 27 μm at the positions of R=0.17 m, 0.18 m, 0.184 m, 0.196 m, and 0.21 m, and the corresponding supergravity coefficients are 158, 143, 130, 122, and 80, respectively, which is inconsistent with the view of Yang et al [12]. Therefore, the possible refining mechanisms for the solidification structure refinement of H13 steel in composite super-gravity fields were explored on the basis of the calculated solidification process via Thermo-Calc software as shown in Fig. 7.

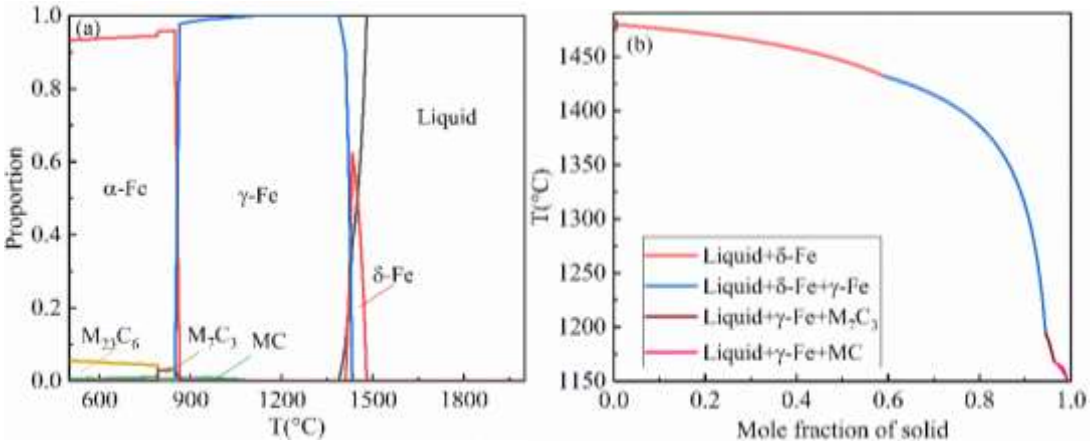

Figure 7. (a) Equilibrium phase diagram and (b) Non-equilibrium phase diagram of H13 steel during solidification (Notes: δ-Fe is high-temperature ferrite; γ-Fe is austenite; α-Fe is ferrite; $M_{23}C_6$, M_7C_3, and MC are carbides' types).

Fig.7(a) is the equilibrium phase diagram of H13 steel during solidification. It can be found that during the solidification of δ-Fe is first precipitated from the liquid phase at 1480 ℃, and then γ-Fe appears in the liquid at 1425 ℃. In fact, the actual solidification process of H13 steel is non-equilibrium. Fig. 7(b) shows the non-equilibrium solidification of H13 steel. The phase of δ-Fe is produced in the temperature range of 1425~1475 ℃, and the corresponding solid phase ratio range is 0-0.6. The phases of δ-Fe and γ-Fe coexist in the temperature range of 1200~1425 ℃, and the stage corresponding to the period that the solid fraction increases from 0.6 to 0.9. When the temperature is less than 1200 ℃, δ-Fe disappears and carbides begin to precipitate, such as M_7C_3 and MC.

During the cooling process of molten steel, δ-Fe is produced in prior to austenite. In general, γ-Fe preferentially nucleates at the grain boundaries of δ-Fe. The energy required for nucleation of γ-Fe is called as the nucleation work, and its value in the supergravity field could be estimated via Eq. (2).

$$\Delta G = -(\Delta G_V + G_g + G_b)V + \sigma A \quad (2)$$

where ΔG is the nucleation energy; ΔG_V is the solid-liquid difference of Gibbs free energy per unit volume; G_g and G_b represent energy per volume exerted on the nucleus provided by normal gravity and super-gravity, respectively, and; σ is the solid-liquid interfacial tension; V is the volume of the solid; and A is the interfacial area.

To simplify the calculation, the following three assumptions are made in this work.

1. Body shrinkage rate ε, surface tension σ (N/m) and the change of chemical potential ΔF_T are independent of super-gravity [9];
2. The change in the chemical potential of the test material was replaced by a change in the Gibbs free energy of the pure iron from 1873 K to 1773 K (0.002575 J/m^3) [16];
3. G_g could be ignored under super-gravity field.

$$\Delta G = -(-\Delta F_T + k\varepsilon p)\frac{4}{3}\pi r^3 + 4\pi r^2\sigma \quad (3)$$

Preprints (www.preprints.org) | NOT PEER-REVIEWED | Posted: 18 September 2020 doi:10.20944/preprints202009.0442.v1

where r is nucleus radius (m); when the temperature is T (K), ΔF_T is change of chemical potential of solidification system (J/m^3, i.e. ΔG_V); k is conversion factor; ε is body shrinkage rate, 0.95 [17]; p is external pressure (N); σ is the solid-liquid interfacial tension (N/m). In the super-gravity field, the external pressure is centrifugal force and can be obtained by calculus. A cubic micro-volume (dR^3) is extracted from the radius R of the liquid metal section, as shown in Fig. 8(a). The particle position of the micro-volume is R-dR/2, and the value of dR is so small that it can be ignored.

During the process of rotation, for the micro-volume element, the centrifugal force and the pressure generated by the radial direction are marked as Eq. (4) and Eq. (5), respectively.

$$\mathrm{d}F = m\omega^2 R = \rho(\mathrm{d}R)^3\omega^2 R \tag{4}$$

$$\mathrm{d}p = \mathrm{d}F \Big/ (\mathrm{d}R)^2 \tag{5}$$

where m is the mass per unit volume (kg); ρ is the density of the liquid metal (kg/m^3). By substituting Eq. (4) into Eq. (5), Eq. (6) can be obtained.

$$\mathrm{d}p = \rho(\mathrm{d}R)^3\omega^2 R \Big/ (\mathrm{d}R)^2 = \rho\omega^2 R\mathrm{d}R \tag{6}$$

The radial integral of p at R,

$$p = \int_{R_0}^{R} \rho\omega R\mathrm{d}R \tag{7}$$

Get

$$p = \rho\omega^2(R^2 - R_0^2)/2 \tag{8}$$

Substituting Eq. (8) into Eq. (3) can results in Eq. (9).

$$\Delta G = \frac{4}{3}\pi \mathrm{r}^3\Delta F_\mathrm{T} - \frac{2}{3}\pi \mathrm{r}^3 \mathrm{k}\varepsilon\rho\omega^2(R^2 - R_0^2) + 4\pi r^2\sigma \tag{9}$$

With the definition of $d\Delta G/dr = 0$, the critical nucleation radius under centrifugal pressure can be calculated by Eq. (9).

$$r^* = 2\sigma/[\mathrm{k}\varepsilon\rho\omega^2(R^2 - R_0^2)/2 - \Delta F_\mathrm{T}] \tag{10}$$

Substituting Eq. (10) into Eq. (9), critical nucleation work (ΔG^*) under centrifugal pressure can result in Eq. (11).

$$\Delta G^* = 16\pi\sigma^3 / \left\{3[\Delta F_\mathrm{T} - \mathrm{k}\varepsilon\rho\omega^2(R^2 - R_0^2)/2]^2\right\} \tag{11}$$

The relationship between critical nucleation work (ΔG^*) and super-gravity coefficient can be expressed in Eq. (12).

$$\Delta G^* = 16\pi\sigma^3 / \left\{3[\Delta F_\mathrm{T} - \mathrm{k}\varepsilon\rho(\mathrm{g}R\sqrt{G^2 - 1} - \omega^2 R_0^2)/2]^2\right\} \tag{12}$$

where k, conversion factor; ε, body shrinkage rate, 0.95; ρ, a solid-liquid two-phase total density calculated by Jmat-Pro softwore, 7.003 kg/m^3; ω, rotational angular speed, rad/s; R, the distance from observation position to centrifugal center (i.e. rotational radius), m; R_0, the inner radius, m.

In literature [9], the calculation method of conversion factor was not mentioned. The effect of conversion factor on the relationship between critical nucleation work and outer radius was discussed. In Fig. 8(b), the abscissa represents the rotational radius and the ordinates on the left and right sides represent the critical nucleation work at k = 1 and k = 100, respectively. At this time, the rotational speed is assumed to be 300 r/min. It can be found that the size of k value can change the

Preprints (www.preprints.org) | NOT PEER-REVIEWED | Posted: 18 September 2020 doi:10.20944/preprints202009.0442.v1

value of ΔG^*, but has no influence on the variation trend of critical nucleation work with rotational radius. Therefore, the value of k was defined as 1.

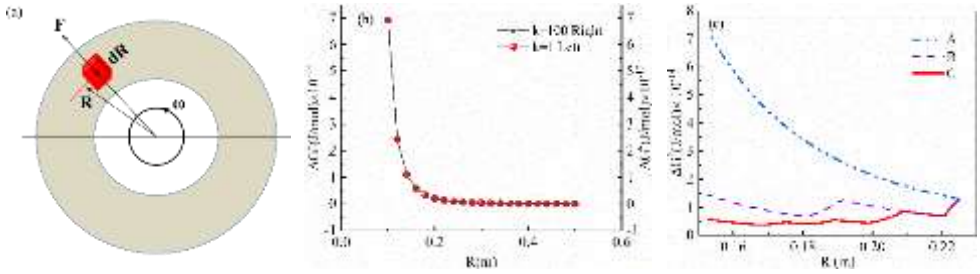

Figure 8. (a) Schematic diagram of centrifugal force analysis (b) Effect of conversion factor (k=1,100) on the relationship between critical nucleation work and outer radius (c) ΔG^* at different positions of Sample A, B, and C.

At the present rotational speed's conditions for Samples A, B, and C, the ΔG^* of Sample A, B, and C were respectively calculated by Eq. (12), as shown in Fig.8 (c). Fig.8 (c) shows that when R decreases from 0.225 m to 0.152 m, the value of ΔG^* for Sample A increases from 1.5×10^{-14} J/mol to 7×10^{-14} J/mol, which means that as R decreases in the supergravity field, the energy required for austenite nucleation increases and the amount of austenite nucleated decreases. Compared with Sample A, the maximum value of ΔG* for Sample B evidently decreases, which makes austenite easy to nucleate. It also can be found that as the value of R decreases, ΔG* decreases at the range of increasing rotational speed, which can be also proved in the variations trend of ΔG* with R in Sample C. In short, during the process of solidification in supergravity field, increasing the number of rotational speeds is beneficial to refine the austenite grains.

In general, γ-Fe easily nucleates on the grain boundaries of δ-Fe during the normal gravity solidification process of steel. The "free" γ dendrites are coarsened and polymerized with the surrounding δ-Fe. Under the same cooling conditions, the degree of polymerization of γ dendrites at the grain boundaries of δ-Fe is significantly higher than that inside the δ-Fe grains. During the cooling process, the dendrites coarsen and compete for growth, thereby forming the dendritic structure. In the super-gravity field, the preferentially precipitated solid phase (dendrite) will undergo centrifugation or centripetal motion, and the dendrite can be broken owing to the difference of density between solid phase and liquid phase. Because of the fracture of dendrites called "fragments", the crystal nuclei are added in the melt causing refinement of solidification structure during casting. This phenomenon is regarded as the "heavy crystal rain" mechanism [6,7,10].

According to Stokes' law [18, 19], the super-gravity coefficient is positively correlated with the moving speed of the solid phase particles, as shown in Eq. (13).

$$\frac{\pi}{6}\mathrm{d}^3(\rho_l-\rho_p)Gg-3\pi\eta\mathrm{d}\frac{ds}{dt}=\frac{\pi}{6}\mathrm{d}^3\rho_p\frac{d^2s}{dt^2} \tag{13}$$

where d is the equivalent diameter of fragment (m); ρ_l and ρ_p are the densities of the liquid and fragment (kg/m^3); η is the dynamic viscosity of the liquid (Pa·s); and s is the displacement of the fragment (m).

When the fragment's movement reaches equilibrium, the right side of Eq. (13) equals zero, and the fragment's moving speed V_r can be expressed as:

$$V_\mathrm{r}=d^2(\rho_l-\rho_p)Gg/18\eta \tag{14}$$

According to Eq. (14), the fragment's moving speed in equilibrium is proportional to the square of its diameter, gravity coefficient and the difference value of solid-liquid two-phase density. The moving speed of dendrite fragments represents the ability of super-gravity to break dendrites, that is, the number of dendritic fragments increases as the moving speed of fragments increases. In the calculation, the equivalent diameter of fragment is 2×10^{-10} m [20], and the viscosity of the molten steel

Preprints (www.preprints.org) | NOT PEER-REVIEWED | Posted: 18 September 2020 doi:10.20944/preprints202009.0442.v1

is 0.0025 Pa·s [21]. According to the calculation results of Jmat-Pro 7.0, the difference value of solid-liquid two-phase density was discussed.

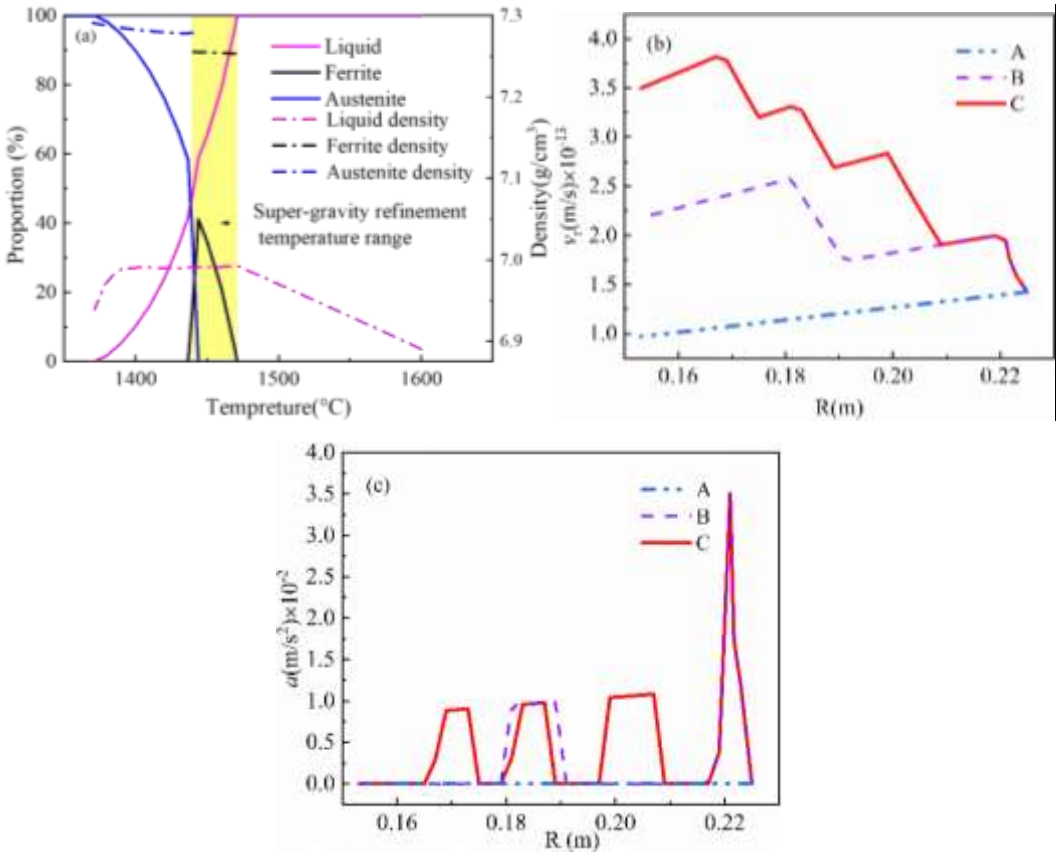

Figure 9. (a) Density change of solid and remaining liquid of H13 steel in the solidification process calculated via Jmatpro7.0 software (b) The fragment's moving speed at different positions of Samples A, B, and C (c) The tangential acceleration at different positions of Samples A, B and C.

In Fig. 9 (a), solid line represents proportion of each phase and dotted line represents density of each phase during solidification. In the initial stage of solidification, the liquid phase ratio is more than 50%, and the solid phase is high temperature ferrite. The density of high temperature ferrite and liquid is 6.98 g/cm^3 and 7.24 g/cm^3, respectively. In the middle of solidification, the liquid phase ratio is less than 50% and greater than 5%, and the solid phase is austenite. The density of austenite and liquid is 6.98 g/cm^3 and 7.28 g/cm^3, respectively. In the end of solidification, the liquid phase ratio is less than 5%, and the solid phase is austenite. The density of austenite slightly elevated but not exceeding 7.3 g/cm^3. The density of liquid decreased to 6.93 g/cm^3 from 6.98 g/cm^3. The super-gravity treatment at the nucleation stage had the best refining effect, while the solidification structures were slightly refined with treatment at the beginning and end of crystal growth [22]. The ranges of refinement super-gravity are solidification fraction less than 59.18 wt% for Al-4.5wt% Cu alloys and 23.16% for Al-8wt% Cu alloys [10]. We assumed that with the liquid phase ratio more than 50% in H13 steel, the super-gravity can refine the solidification structure. Within this range, the difference value of ρ_l and ρ_p almost unchanged, and the value of ρ_l - ρ_p is defined as 0.26 g/cm^3. The moving speed of fragment was calculated by the crystal rain mechanism is shown in Fig. 9 (b).

Fig. 9 (b) shows the relationships between v_r and R for Samples A, B, and C. As R decreases from 0.225 m to 0.153 m, the value of v_r for Sample A decreases from 1.4×10^{-13} m/s to 1.0×10^{-13} m/s. For Samples B and C, v_r increases with the decrease of R at the range of increasing rotational speed, which leads to the reduction of secondary dendrite spacings. For Samples B and C, the variations trends of secondary dendrites spacings with R are opposite to the variation trends of v_r with R. If the refinement mechanism of dendritic structure only is the "heavy crystal rain" mechanism, the difference of SDAS depends on that of v_r. Combining with Fig.6 (a), the differences of SDAS between R=0.225 m and

Preprints (www.preprints.org) | NOT PEER-REVIEWED | Posted: 18 September 2020 doi:10.20944/preprints202009.0442.v1

R=0.152 m for Samples A and C are respectively 50 μm and 24 μm, and the corresponding differences of v_r between R=0.225 m and R=0.152 m for Samples A and C are respectively 0.5×10^{-13} m/s and 3.2×10^{-13} m/s. Obviously, the values of SDAS is not completely related to v_r, which means that other mechanism has effect on SDAS.

In the process of super-gravity casting, the tangential force is generated by the increase or decrease of the rotational speed of the mold, which will change the motion state of the molten metal and break the dendrites, thus refining the solidification structure. This refinement of solidification structure is called dynamic effect [23, 24]. The dynamic effect on the movement state of molten metal can be explained by the Reynolds number (Re) formula of fluid mechanics. For centrifugal casting, the Reynolds number can be expressed as Eq. (15)

$$\mathrm{Re}—vb/\nu \tag{15}$$

where, v is the average linear speed of the liquid relative to the mold; b is the thickness of the liquid layer in the mold; ν is the kinematic viscosity coefficient of the liquid. In the super-gravity casting process, v quickly becomes smaller, and Re becomes smaller. At the moment, the flow of the liquid steel to the inner wall of the mold is laminar, and the crystal front is in the laminar layer, which will promote the precipitation of small grains along the solid-liquid interface in one direction, thus forming inclined columnar crystals.

After the implementation of the dynamic effect, both v and Re increase significantly. If Re is greater than a certain value, the flow of liquid steel against the inner wall forms a turbulent layer. The crystallization front is in the turbulent layer, which hinders the normal floating and sinking of the heterogeneous particles. This results in the chaotic motion of particles at different temperatures in the whole turbulent layer, which reduces the temperature difference between the liquid layers, and accelerates the melting of the dendrites, thus promoting the transformation of columnar crystals into equiaxed crystals. In the dynamic effect, the tangential force F acting on the dendrite vertex and breaking the dendrite can be expressed as:

$$F=m\cdot a \tag{16}$$

where m is the mass of the liquid layer at the dendrite front; a is the tangential acceleration of the dendrite front, which is determined by the angular acceleration of the liquid layer (ω_a) and the distance from its center of gravity to the axis of rotation (R)

$$a=\omega_a\cdot R \tag{17}$$

If the angular speed of the dendritic liquid layer relative to the solidified layer changes by Δω during Δt, then

$$\omega_a=\Delta\omega/\Delta\mathrm{t} \tag{18}$$

By combining Eq. (17), and (18), the following Eq. (19) can be obtained:

$$F=\Delta\omega/\Delta\mathrm{t}\cdot R\cdot m \tag{19}$$

When F is greater than a certain value sufficient to break the crystallization front dendrites, the crystallization front will form dendritic fragments that act as the nuclear cores of the grains. Tangential acceleration of the liquid layer at the dendrite front (a) is expressed as Eq. (20).

$$a=30\pi\Delta N/\Delta\mathrm{t}\cdot R \tag{20}$$

It can be found that the fragment's tangential acceleration is caused by the change of rotational speed. When the angular acceleration in the super-gravity field is a fixed value, the tangential acceleration of the fragment is positively correlated to the radius.

Fig.9 (c) shows the tangential accelerations of the dendrites front for Samples A, B, and C. As shown by the blue dotted line in Fig. 9 (c), the value of a at each position of Sample A is zero, which demonstrates there is not dynamic effect mechanism in Sample A. The value of a is not zero at the range of increasing rotational speed. The value of a is proportional to R, and a at R=0.22 m is much more than that at other positions such as R=0.22 m, 0.203 m, 0.185 m, and 0.17m. Compared with

Preprints (www.preprints.org) | NOT PEER-REVIEWED | Posted: 18 September 2020 doi:10.20944/preprints202009.0442.v1

Sample B, there is much more positions of $a>0$ for Sample C, which leads that at the same position, the value of SDAS is smallest in Sample C.

In summary, the refinement mechanisms of solidification microstructure for H13 steel in supergravity field include the lower critical nucleation work, the "crystal rain" mechanism, and the dynamic effect mechanism. Among them, the "crystal rain" mechanism does not contribute much more to the refinement effect of H13 solidification structure than binary alloy such as Al-Cu alloys. The reason is that during the solidification in supergravity fields, the density difference between the solid and liquid phases is an important factor in the generation of dendritic rain, and compared with the density difference between the solid and liquid phases of the Al-Cu alloy (i.e. 0.9 g/cm^3), the density difference between the solid and liquid phases of H13 (0.27 g/cm^3) is smaller.

3.3. Tensile Properties of As-cast H13 Samples in Super-gravity Fields

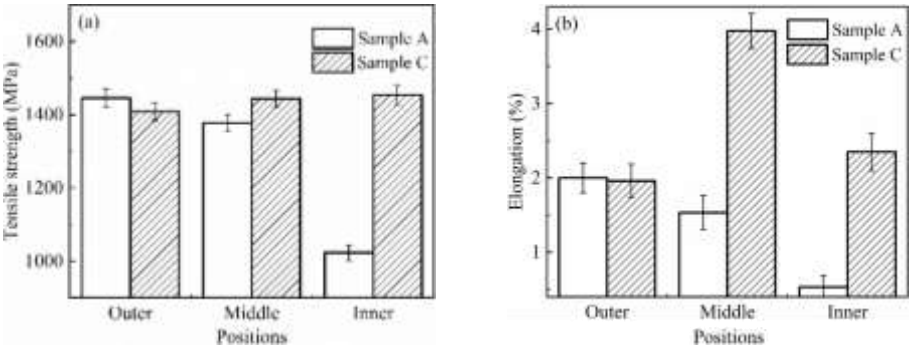

Figure 10. Tensile strength (a) and Elongation (b) at outer, middle, and inner of Samples A and C.

The tensile strength and elongation at room temperature for the as-cast H13 samples are shown in Fig. 10. It is clear that the tensile strengths and elongations of Samples A and C are basically equal at outer positions. However, the tensile strength and elongation of Sample C are significantly larger than Sample A at positions of middle and inner, especially for the elongation. It is well-known that the decrease in grain size can increase both the strength and the plasticity [25, 26]. In the present study, the grain size at inner position decreases with the increasing rotational speeds as clearly shown in Fig. 6, as a result of which, both the strength and plasticity are enhanced remarkably. Therefore, it is well demonstrated that multi-rotational speeds supergravity field can effectively enhance both the strength and plasticity of the as-cast H13 steel through decreasing the grain size.

. 5.Conclusion

The grain refinement and tensile properties of as-cast Cu-Sn alloys in multi-rotational speeds supergravity field were investigated. The conclusions drawn are as follows:

(1) The solidification structure of H13 steel can be significantly refined in multi-rotational speeds super-gravity field.

(2) The decrease of critical nucleation work for austenite in multi-rotational speeds supergravity field promotes the grain multiplication, resulting in the refinement of austenite grain size. The tangential force produced by the change of the rotational speed in the supergravity field breaks dendrites at the solidification front and causes the solidification structure refinement finally. Due to the smaller density difference between the solid and liquid phases of H13 steel, the "crystal rain" mechanism does not contribute much more to the refinement effect of H13 solidification structure than binary alloys.

(3) The increasing supergravity can greatly enhance the tensile properties of as-cast H13 steel through refining austenite grains size and secondary dendrites. Both the tensile strength and plasticity at inner position of supergravity samples are greatly enhanced with the increasing rotational speed.

Acknowledgements

The authors are thankful for the support from the Science and Technology Program of Sichuan Province, China (Grant NO. 18SYXHZ0069), and the Beijing Key Laboratory of Special Melting and Preparation of High-End Metal Materials in the School of Metallurgical and Ecological Engineering of University of Science and Technology Beijing, China.

References

[1] J. Zhu, Z.H. Zhang and J.X. Xie, *Mater. Sci. Eng. A*, 752, 101-114 (2019).

[2] H. Zhou, H. F. Zhang, X. Tong, D.L. Cong, C. W. Wang and L.Q. Ren, *Mater. Des.* 51: 886-893 (2013).

[3] W. Kurz, D.J. Fisher, J.G. Li and Q.D. Hu. Fundamentals of Solidification, 4th ed. (Bei Jing, B J: Higher education press), pp. 71-73.

[4] C. Cicutti and R. Boeri, *Scr. Mater.* 45, 1455-1460 (2001).

[5] A.F. Ferreira, E.G. Melo and L.O. Ferreira, *Steel Res. Int.*, 86, 58-64 (2015).

[6] X. Liao, Q. Zhai, J. Luo, W. Chen and Y. Gong, *Acta Mater.*, 55, 3103-3109 (2007).

[7] Y.Y. Gong, J. Luo, J. X. Jing, Z.Q. Xia and Q.J. Zhai, *Mater. Sci. Eng. A*, 497, 147-152 (2008).

[8] F.P. Qi, H.B. Zhang, S. L. Gao and Q.J. Zhai, *Journal of Shanghai University (English Edition)*, 9, 74-77 (2005).

[9] S.J. Jia, B. Song, G.Y. Song, Y.H. Yang and C.G. Huang, *The Chinese Journal of Process Engineering*, 14, 881-885 (2014).

[10] Y.H. Yang, B. Song, Z.B. Yang, G.Y. Song, Z.Y. Cai and Z.C. Guo, *Materials*, 9, 1001-1014 (2016).

[11] L. X. Zhao, Z. C. Guo, Z. Wang and M.Y. Wang, *Metall. Mater. Trans. A*, 41, 670-675 (2010).

[12] Y.H. Yang, B. Song, Z.B. Yang, J. Cheng, G.Y. Song, L.F. Li. *Metall. Res. Technol.* 115, 1-12 (2018).

[13] Y.H. Yang, B. Song, J. Cheng, G.Y. Song, Z.B. Yang, Z.Y. Cai. *ISIJ Int.*, 58, 98-106 (2018).

[14] Z. H. Melgarejo, O. M. Suárez and K. Sridharan. *Composites, Part A*, 39, 1150-1158 (2008).

[15] X.K. Liu, Q.S. Wang, Z.D. Wang, Z.Q. Feng, H. Zhang, J.J. Zhu and M. Fan, *Foundry (Chinese)*, 4, 351-354 (2010).

[16] I. Barin, O. Knacke and O. Kubaschewski, Thermochemical Data of Pure Substances, 3rd ed. (Berlin, BER: Springer, (2008), p.675.

[17] X.C. Chen. New Process Development and Finite Element Simulation of Induction Electroslag Centrifugal Casting, University of Science and Technology Beijing, Beijing, 2001.

[18] Y. Watanabe, Y. Inaguma, H. Sato and Miura F., *Materials*, 2, 2510-2525 (2009).

[19] Y. Watanabe, A. Kawamoto and K. Matsuda, *Compos. Sci. Technol.*, 62, 881-888 (2002).

[20] Z.Q. Cui and Y.C. Qin. Metal Science and Heat Treatment, 2nd ed. (Beijing, BJ: China Machine Press), p.39.

[21] J.X. Chen. General Steelmaking Chart Data Sheet, 2nd ed. (Bei Jing, B J: Higher education press), p. 534.

[22] Y.H. Yang. Fundamental Study on Solidification Structure Refinement and Elements Segregation of Metals by Super Gravity, University of Science and Technology Beijing, Beijing, 2017.

[23] G.W. Lin, Z.B. Li and M.T. Cheng, *Foundry (Chinese)*, 1, 1-7 (1998).

[24] G.W. Lin, Z.B. Li and M.T. Cheng, *Iron and steel (Chinese)*, 32, 21-25 (1997).

[25] H. S. Jiang, M. Y. Zheng, X. G. Qiao, K. Wu, Q. Y. Peng, S. H. Yang, Y. H. Yuan and J. H. Luo: *Mater. Sci. Eng. A*, 684 158-164 (2017).

[26] B. Pourbahari, H. Mirzadeh and M. Emamy: *Mater. Sci. Eng. A*, 680, 39-46 (2017).